



Contents lists available at ScienceDirect

Journal of Controlled Release

journal homepage: www.elsevier.com/locate/jconrel

Focused ultrasound combined with microbubble-mediated intranasal delivery of gold nanoclusters to the brain



Dezhuang Ye^{a,1}, Xiaohui Zhang^{b,1}, Yimei Yue^c, Ramesh Raliya^d, Pratim Biswas^d, Sara Taylor^e, Yuan-chuan Tai^b, Joshua B. Rubin^{e,f}, Yongjian Liu^b, Hong Chen^{c,g,*}

^a Department of Mechanical Engineering and Material Science, Washington University in St. Louis, Saint Louis, MO 63130, USA

^b Mallinckrodt Institute of Radiology, Washington University School of Medicine, St. Louis, MO 63110, USA

^c Department of Biomedical Engineering, Washington University in St. Louis, Saint Louis, MO 63130, USA

^d Department of Energy, Environmental & Chemical Engineering, Washington University in St. Louis, Saint Louis, MO 63130, USA

^e Department of Pediatrics, Washington University School of Medicine, St. Louis, MO 63110, USA

^f Department of Neuroscience, Washington University School of Medicine, St. Louis, MO 63110, USA

^g Department of Radiation Oncology, Washington University School of Medicine, Saint Louis, MO 63108, USA

ARTICLE INFO

Keywords:

Focused ultrasound
Nanoparticle
Intranasal delivery
Blood-brain barrier
Positron emission tomography
Brain drug delivery
Brainstem

ABSTRACT

Focused ultrasound combined with microbubble-mediated intranasal delivery (FUSIN) is a new brain drug delivery technique. FUSIN utilizes the nasal route for direct nose-to-brain drug administration, thereby bypassing the blood-brain barrier (BBB) and minimizing systemic exposure. It also uses FUS-induced microbubble cavitation to enhance transport of intranasally (IN) administered agents to the FUS-targeted brain location. Previous studies have provided proof-of-concept data showing the feasibility of FUSIN to deliver dextran and the brain-derived neurotrophic factor to the caudate putamen of mouse brains. The objective of this study was to evaluate the biodistribution of IN administered gold nanoclusters (AuNCs) and assess the feasibility and short-term safety of FUSIN for the delivery of AuNCs to the brainstem. Three experiments were performed. First, the whole-body biodistribution of IN administered ⁶⁴Cu-alloyed AuNCs (⁶⁴Cu-AuNCs) was assessed using *in vivo* positron emission tomography/computed tomography (PET/CT) and verified with *ex vivo* gamma counting. Control mice were intravenously (IV) injected with the ⁶⁴Cu-AuNCs. Second, ⁶⁴Cu-AuNCs and Texas red-labeled AuNCs (TR-AuNCs) were used separately to evaluate FUSIN delivery outcome in the brain. ⁶⁴Cu-AuNCs or TR-AuNCs were administered to mice through the nasal route, followed by FUS sonication at the brainstem in the presence of systemically injected microbubbles. The spatial distribution of ⁶⁴Cu-AuNCs and TR-AuNCs were examined by autoradiography and fluorescence microscopy of *ex vivo* brain slices, respectively. Third, histological analysis was performed to evaluate any potential histological damage to the nose and brain after FUSIN treatment. The experimental results revealed that IN administration induced significantly lower ⁶⁴Cu-AuNCs accumulation in the blood, lungs, liver, spleen, kidney, and heart compared with IV injection. FUSIN enhanced the delivery of ⁶⁴Cu-AuNCs and TR-AuNCs at the FUS-targeted brain region compared with IN delivery alone. No histological-level tissue damage was detected in the nose, trigeminal nerve, and brain. These results suggest that FUSIN is a promising technique for noninvasive, spatially targeted, and safe delivery of nanoparticles to the brain with minimal systemic exposure.

1. I. Introduction

The development of effective therapies for central neural system (CNS) diseases is often challenged by the blood-brain barrier (BBB), which prevents most therapeutic compounds from reaching the brain at

the therapeutic level [1]. Current clinical strategies to circumvent the BBB are either invasive (e.g., Gliadel wafers, intrathecal injection, and convection-enhanced delivery) or lack specific targeting to the diseased site (e.g., hyperosmolar disruption using mannitol and intranasal brain drug delivery) [2]. The use of focused ultrasound (FUS) and

* Corresponding author at: Department of Biomedical Engineering and Department of Radiation Oncology, Washington University in St. Louis, 4511 Forest Park Ave., St. Louis, MO 63108, USA.

E-mail address: hongchen@wustl.edu (H. Chen).

¹ Dezhuang Ye and Xiaohui Zhang contributed equally.

<https://doi.org/10.1016/j.jconrel.2018.07.020>

Received 20 March 2018; Received in revised form 5 June 2018; Accepted 11 July 2018

Available online 26 July 2018

0168-3659/ © 2018 Elsevier B.V. All rights reserved.

microbubbles to enhance the BBB permeability is a recently developed technique for noninvasive and localized delivery of intravenously (IV) injected drugs [3, 4]. However, the goals of drug delivery are not only to increase the local drug delivery efficiency but also to reduce systemic toxicity. Despite the great promise of the FUS-induced BBB opening technique, systemic drug toxicity associated with IV injection remains a clinical challenge. Brain drug delivery strategies that can circumvent the BBB for noninvasive and localized drug delivery with minimized systemic exposure are greatly needed to improve the treatment of CNS diseases. FUS in combination with microbubble-mediated intranasal delivery (FUSIN) has the potential to address this need. FUSIN is a novel technique first introduced by Chen and Konofagou in 2014 [5]. It utilizes the nasal route for direct nose-to-brain drug administration, thereby bypassing the BBB and minimizing systemic exposure. It also uses FUS-induced microbubble cavitation to enhance the transport of IN administered agents to the FUS-targeted brain location.

The IN route can deliver therapeutic agents directly from the nose to the brain through the olfactory and trigeminal nerve pathways, bypassing the BBB and minimizing systemic exposure [6]. Direct IN delivery of therapeutics to the brain was first proposed in the 1980s [7]. The exact mechanisms underlying IN brain drug delivery are not entirely understood; however, two pathways have been identified: the olfactory nerve pathway and trigeminal nerve pathway [6]. IN administered therapeutics can be transported from the nasal cavity to the brain along the olfactory nerve and trigeminal nerve, which innervate the epithelium of the nasal passages and enter the brain in the olfactory bulb and pons, respectively. Once inside the brain entry points (*i.e.*, olfactory bulb and brainstem), the IN administered agents are distributed in the whole brain along the cerebral perivascular spaces – thin annular regions surrounding the blood vessels – and may be propelled through the perivascular spaces by heartbeat-driven pulsations of the blood vessel walls, called the “perivascular pump effect” [8]. A wide-range of therapeutics, such as peptides, proteins, gene vectors, and stem cells, have been successfully delivered to the brain through IN administration and have shown efficacy in treating CNS diseases in small animal models [9–12]. IN insulin delivery for the treatment of patients with Alzheimer's disease has been tested in early-phase clinical trials [13, 14]. Recently, new formulations and delivery approaches have been developed to further enhance the nose-to-brain transport efficiency, mainly with the use of nanoparticles as drug carriers [15–17, 36]. However, IN brain drug delivery remains limited to preclinical studies and small early-phase clinical trials [18–21] mainly because the delivery is inefficient and not diseased-site targeted [19].

Unlike the more established FUS-induced BBB opening technique for trans-BBB delivery of therapeutics in the systemic circulation, FUSIN uses FUS to activate microbubbles at a targeted brain location to enhance the local accumulation of IN administered agents that are already beyond the BBB. Previous studies showed that FUSIN enhanced the delivery of IN-administered dextran and a protein drug (brain-derived neurotrophic factor, BDNF) at the FUS-targeted caudate putamen of mouse brains [5, 22]. Based on our previous work on ultra-high-speed photomicrography of microbubble dynamics in *ex vivo* microvessels [23], we observed that microbubble oscillations push and pull on the blood vessel, which leads to expansion and contraction of the vessel and surrounding tissue. Based on the similarity of this phenomenon with the perivascular pump effect, we hypothesized that the “microbubble pump effect” may be the potential mechanism for FUSIN. This mechanism was indirectly verified by comparing the delivery efficiency of FUS sonication before IN administration (without the microbubble pump effect) to FUS after IN administration (with the microbubble pump effect) [22]. It was found that significant enhancement was observed only when FUS sonication was performed after IN, suggesting that the microbubble pump effect contributes to FUSIN.

The objective of this study was to evaluate the biodistribution of IN administered gold nanoclusters (AuNCs) and assess the feasibility and short-term safety of FUSIN for the delivery of AuNCs to the brainstem.

Ultrasmall nanoclusters have drawn significant attention for biomedical applications due to their size-promoted clearance after systematic injection [24–28], and accurate tumor targeting as we demonstrated in previous research [29]. We have previously reported on renal clearable AuNCs integrated with ^{64}Cu (^{64}Cu -AuNCs) which showed minimal nonspecific organ retention, largely reduced mononuclear phagocytosis system accumulation, and precise detection of cancer biological targets in both primary tumor and distant metastasis using positron emission tomography (PET) [29]. Meanwhile, their sizes were close to that of monoclonal antibodies, which are used with increasing success against many tumors [30]. The first-in-human trial is now ongoing to determine the safety of small-size gold nanoparticles (13 nm in diameter) labeled with spherical nuclei acid in treating patients with recurrent glioblastoma or gliosarcoma (ClinicalTrials.gov Identifier: NCT03020017).

We selected the brainstem as the targeted brain location because our long-term goal is to use FUSIN for the treatment of diffuse intrinsic pontine glioma (DIPG). DIPG, a high-grade glioma that spreads throughout the brainstem, has replaced leukemia as the leading cause of cancer death among children. It has a median survival of less than one year, a dismal prognosis that has remained unchanged over the past 40 years [31]. There are two main reasons why treatment of DIPG is challenging. First, in contrast to other high-grade gliomas (*e.g.*, glioblastoma), which often have a compromised BBB, the BBB in DIPG is frequently intact, as suggested by the lack of contrast enhancement on contrast-enhanced magnetic resonance imaging [32]. Second, the brainstem controls basic life functions, such as breathing, hearing, taste, balance, and communication between different parts of the brain. The critical anatomic location of the brainstem precludes surgical intervention and limits the use of other invasive therapeutic techniques. Therefore, techniques that can noninvasively circumvent the BBB can have a significant clinical impact in treating DIPG. FUSIN has the potential to improve DIPG treatment by bypassing the BBB and addressing the critical need, shared by many pediatric brain diseases, for non-invasive and targeted delivery of therapeutics to the diseased brain site, while minimizing injury to healthy regions of the developing brain and other organs. In addition, the brainstem is also unique in that it is directly connected with the nasal cavity through the trigeminal nerve. Our previous studies showed that FUSIN delivered different agents to the caudate putamen [5, 22]. This study explored the potential to expand the application of FUSIN for drug delivery to the brainstem.

2. Materials and methods

2.1. Animals

All animal procedures were reviewed and approved by the Institutional Animal Care and Use Committee of Washington University in St. Louis, in accordance with the National Institutes of Health Guidelines for animal research. C57BL/6 female mice (6–8 weeks, ~25 g body weight) were purchased from Charles River Laboratory (Wilmington, MA, USA). The animals were housed in a room maintained at 72 °F and 55% relative humidity, with a 12-h/12-h light/dark cycle, and provided access to standard laboratory chow and tap water. Mice were divided into multiple groups (Table 1).

2.2. Synthesis and characterization of AuNCs

^{64}Cu -AuNCs were synthesized as described previously [28]. In a typical reaction, water (2.0 mL), HAuCl_4 (10 mM, 376 μL), and $^{64}\text{CuCl}_2$ (74 MBq) were mixed in a glass vial, followed by the dropwise addition of mPEG-lipoamide (MW = 750 Da, 10 mM, 400 μL). After the mixture was stirred overnight, sodium borohydride (40 mM, 400 μL) was added and stirred rapidly for 2 h. The ^{64}Cu -AuNCs were collected by first filtering the solution through an Amicon 50 K centrifuge filter and subsequently purifying the solution with an Amicon 10 K centrifuge filter.

Table 1
Summary of all study groups.

Study	Groups	Analysis
Biodistribution of IN vs. IV administered AuNCs	1 ⁶⁴ Cu-AuNCs + IN (n = 4) ⁶⁴ Cu-AuNCs + IV (n = 4)	PET and gamma counting
Feasibility of FUSIN for the delivery of AuNCs	2 ⁶⁴ Cu-AuNCs + FUSIN (n = 5) ⁶⁴ Cu-AuNCs + IN (n = 3)	Autoradiography
Short-term safety of FUSIN	3 TR-AuNCs + FUSIN (n = 3)	Fluorescence imaging
	4 Non-treated control (n = 3) TR-AuNCs + IN (n = 3); Sacrificed 1 h post IN TR-AuNCs + IN (n = 3); Sacrificed 24 h post IN	Fluorescence imaging of the nasal tissue and trigeminal nerve
	5 Non-treated control (n = 3) TR-AuNCs + FUSIN (n = 3)	Histological staining of the nasal tissue, trigeminal nerve, and brain

Radiochemical purity was determined using silica impregnated iTLC paper with a mobile phase of 1:1 methanol: 10% ammonium acetate. The synthesis and purification procedures for the Texas red-labeled AuNCs (TR-AuNCs) was similar to the above procedures with the addition of 5% (molar fraction) lipoamido-dPEG₁₂-Texas red in 10 μ L dimethyl sulfoxide to the solution after the addition of mPEG-lipoamide to H₂SO₄ and stirred in darkness. Same as that reported in our previous publication [28], the prepared AuNCs had a homogenous distribution as characterized by transmission electron microscopy (Tecnaï G2 Spirit Transmission Electron Microscope, Hillsboro, OR). Dynamic light scattering (Zetasizer Nano ZS, Malvern Instruments, Malvern, UK) measurements found their hydrodynamic sizes were 5.60 ± 1.50 nm.

2.3. IN administration

The IN administration procedure was the same as described before [5]. Mice were placed supine on a curved holder under 1.5% isoflurane anesthesia. Drops (3 μ L for each drop) of AuNCs suspended in saline solution was administered to the mouse nose by alternating between the left or right nostril every 2 mins. Those drops were placed at the opening of the nostril, allowing the animal to snort each drop into the nasal cavity. A total of 8 drops (24 μ L) were administered to each mouse. The administered AuNC dose was ~ 4 mg/kg mouse body weight.

2.4. Biodistribution evaluation of IN administration

One group of mice (n = 4) were administered with ⁶⁴Cu-AuNCs (3.7 MBq/mouse) through IN administration. The other group of mice (n = 4) was intravenously injected with ⁶⁴Cu-AuNCs (3.7 MBq/mouse) through the tail vein. *In vivo* PET/CT scans were performed using the Inveon PET/CT system (Siemens, Malvern, PA) at 1 h post IN administration or IV injection. The PET images were corrected for attenuation, scatter, and camera dead time, and were co-registered with the CT images. The PET images were reconstructed with the maximum *a posteriori* (MAP) algorithm using Inveon software. After PET imaging, blood was collected from the mouse heart, and each mouse was transcardially perfused with phosphate-buffered saline followed by 4% paraformaldehyde. All the major organs were harvested after perfusion. Then, the collected blood and organs were placed in tested tubes, weighed, and counted using a Beckman 8000 gamma counter (Beckman, Fullerton, CA). The count rate (counts per minute, CPM) for each sample was corrected by automatic background subtraction and decay correction (compensate for the decay of ⁶⁴Cu radioactivity over time). The corrected CPM from each tissue sample was then normalized to both the mass of the tissue sample (in grams, g) and the injected dose (ID) for the quantification of ⁶⁴Cu-AuNCs biodistribution in terms of % ID/g. The above study was performed by trained technicians at the Pre-clinical PET/CT Imaging Facility at Washington University in St. Louis.

2.5. FUSIN treatment

Two FUS systems, one for the delivery of non-radiolabeled AuNCs and the other for the delivery of ⁶⁴Cu-AuNCs, were used in this study. The second system was needed as it was placed in a room approved for the use of radioactive materials and dedicated for the delivery of radioactive ⁶⁴Cu-AuNCs. Both systems were carefully calibrated using a needle hydrophone (HGL-0200, Onda Corporation, Sunnyvale, CA, USA) to ensure consistent output from these two systems.

The first FUS system (VIFU 2000; Alpinion US Inc., Bothell, WA, USA) consisted of a FUS transducer with a center frequency of 1.5 MHz, a focal depth of 60 mm, an aperture of 60 mm, and a circular central opening of 38 mm. The transducer was mounted to a 3D stage for precise positioning (Velmex, Lachine, QC, Canada). The transducer was attached to a water balloon filled with degassed water to provide acoustic coupling. The water balloon was immersed in a degassed water container, the bottom of which featured a window sealed with an acoustically and optically transparent membrane (Tegaderm; 3M, St. Paul, MN, USA). A B-mode imaging probe (L8-17, working frequency 8–17 MHz, center frequency 12 MHz, Alpinion, Seoul, Korea) was inserted into the FUS transducer center opening and aligned with the FUS focal plane. Treatment planning was executed with the assistance of a grid [33]. The grid was positioned in the water container on top of the mouse head with the crossing point in alignment with the lambda, an anatomic landmark on the skull that is visible through the mouse skin on the head. The B-mode imaging probe was scanned through the grid to form a 3D image of the grid using a customized Matlab (R2016b; Mathworks inc., Natick, MA, USA) program. The crossing point of the grid was then identified and used as the reference point to align the FUS focus at one selected point on the left side of the brainstem based on its stereotactic location relative to the lambda (0 mm frontal and 1.5 mm to the left). The depth of the FUS focus was adjusted to be 4.0 mm from the skull by measuring the distance from the skull on the B-mode images.

The second system used a FUS transducer (University of Texas Southwestern, Dallas, TX, USA) with an aperture of 75 mm and a radius of curvature of 60 mm. The transducer was impedance-matched to operate at 1.5 MHz, the same as the first system. The transducer was driven by an arbitrary waveform generator (Agilent 33500B; Agilent Technologies, Loveland, CO, USA) connected to a power amplifier (1020 L; E&I, Rochester, NY, USA). The function generator was controlled by a customized MATLAB program. A stereotactic apparatus (Kopf, Tujunga, CA, USA) was used for targeting the brainstem [34]. A pointer was fixed on the stereotactic frame and well characterized to indicate the focus of the transducer. After aligning the tip of the pointer with the lambda, the pointer was then replaced by the FUS transducer, and the transducer was moved to target the brainstem based on the stereotactic location of the brainstem.

The pressure amplitudes and beam profiles of the two FUS transducers were calibrated using a needle hydrophone in a degassed water tank before the experiment. The reported pressure amplitudes were

corrected for 18% mouse skull attenuation [33]. The axial and lateral full-width-at-half-maximum (FWHM) focal regions of the FUS transducer in the first system were 6.04 mm and 0.62 mm, respectively. The FWHM dimensions of the FUS transducer in the second system were 8.62 mm and 1.00 mm, respectively.

For the FUSIN treatment using both systems, AuNCs were administered to the mice before placing the mice prone on a heating pad with their heads immobilized by the stereotaxic frame. The fur on the mouse head was removed while the skull and the scalp remained intact. The water container was placed on the mouse head and coupled with degassed ultrasound gel. The FUS transducer was then adjusted to target the brainstem, using the method described above. Microbubbles comprised of a liquid shell made of 90 mol% 1,2-distearoyl-sn-glycero-3-phosphocholine (DSPC, Avanti Polar Lipids, Alabaster, AL) and 10 mol% 1,2-distearoyl-sn-glycero-3-phosphoethanolamine-N-[methoxy(polyethylene glycol)-2000] (DSPE-PEG2000, Avanti Polar Lipids, Alabaster, AL) and a perfluorobutane gas core (FluoroMed, Round Rock, TX) were manufactured in-house according to a previously described protocol [22]. Size-selected microbubbles with a median diameter of 4–5 μm were isolated from a polydispersed microbubble distribution using a differential centrifugation method [22] and diluted using sterile saline to a final concentration of approximately 8×10^8 number of microbubbles per mL. The diluted microbubbles (volume = 30 μL) were administered through a bolus injection via the tail vein. Immediately (~ 9 s) following microbubbles injection, FUS treatment was performed using the following parameters: peak-negative pressure = 0.56 MPa, pulse length = 6.7 ms, pulse repetition frequency = 5 Hz, and duration = 1 min.

2.6. Spatial distribution of the delivered ^{64}Cu -AuNCs in the brain

^{64}Cu -AuNCs were delivered to mice in the IN-only group ($n = 3$) and FUSIN group ($n = 5$). All the mice were transcardially perfused at 1 h post-IN administration. The excised brains were sliced into 2-mm coronal sections using a brain matrix (RBM-2000C; ASI Instruments, Inc., Warren, MI, USA). The slices were placed on a phosphor-imaging plate for overnight exposure. The radioactivity of the brain slices was detected by autoradiography [35] using a Storm 840 Phosphorimager (GE, Marlborough, MA). The FUS-treated brain slices were selected and quantified using ImageJ (NIH, Bethesda, MD, USA) by calculating the total radioactivity of those slices. The radioactivity of the corresponding slices acquired from mice in the IN only group was also quantified for comparison.

2.7. Spatial distribution of the delivered TR-AuNCs in the brain

TR-AuNCs were intranasally administered to mice ($n = 3$) and FUS treatment was targeted at the left side of the brainstem with the contralateral right side of the brainstem used as the control for IN administration only. The animals were transcardially perfused at 1 h post-IN administration. The mouse brains were harvested and fixed overnight in paraformaldehyde followed by cryoprotection with sucrose. The brains were cut into horizontal sections (the thickness of each section was 60 μm) and imaged using a fluorescence microscope (Axiovert S100; Zeiss, Oberkochen, Germany). For each mouse, a customized Matlab program was used to quantify the fluorescence intensities of 12 sequential brain slices acquired at the targeted brain location [37]. Circles with a 2-mm diameter were selected by the Matlab program on the left and right sides of the brainstem as the regions of interests (ROIs). Another circle was drawn outside of the brain for the calculation of the mean background image intensity. The sum of the pixel intensities within each ROI was normalized by the mean background image intensity of each slice. The average of the normalized fluorescence intensities within the left and right ROIs of the 12 sequential slices was calculated to represent the fluorescence intensities of the FUSIN-treated and IN-treated brain tissues for each mouse, respectively.

2.8. TR-AuNCs distribution in the nose and nerve

TR-AuNCs were intranasally delivered to six mice, three of them were sacrificed at 1 h ($n = 3$), and the remaining three were sacrificed at 24 h ($n = 3$). The nasal tissue and trigeminal nerves were carefully extracted from these two groups of mice. They were examined using a fluorescence imaging system (Bruker Corporation, Billerica, MA). Tissues from mice ($n = 3$) without TR-AuNCs administration were used as the control. The exposure time for the fluorescence imaging was kept the same for all samples.

2.9. Histological analysis

Histologic examinations of the mouse whole brain, nose, and trigeminal nerve were performed to verify the short-term (1 h after treatment) safety of FUSIN. The harvested mouse brains were fixed in 4% paraformaldehyde and embedded in paraffin. The brains were sectioned horizontally into 6 μm thick slices at 10 separate levels, with 180 μm intervals between two adjacent levels. At each level, four sections were acquired and stained with Hematoxylin and eosin (H&E). The mouse noses were immersed overnight in a decalcifying solution before paraffin embedding. The nasal tissue was also sectioned into 6 μm thicknesses and then stained with H&E. The trigeminal nerves were fixed overnight in paraformaldehyde followed by cryoprotection with sucrose, then sectioned into 10 μm sections and stained with Luxol fast blue-cresyl violet (LFB-CV). Histological evaluation was performed single-blinded, by a trained observer without knowledge of the location and parameters of sonication.

2.10. Statistical analysis

Statistical analysis was performed using GraphPad Prism (Version 5.01, La Jolla, CA, USA). Group variation was described as the mean \pm standard deviation. Differences between two groups were determined using the unpaired two-tailed Student's *t*-test. A *p*-value < 0.05 was considered to represent a significant difference.

3. Results

3.1. IN administration minimized systemic exposure

Fig. 1 compares the whole-body biodistribution of ^{64}Cu -AuNCs at 1 h after IN administration and IV injection. The PET/CT image of a mouse administrated with ^{64}Cu -AuNCs via IV route (Fig. 1A) shows the distribution of ^{64}Cu -AuNCs in multiple organs, while the radioactivity was only clearly observed in the nose, stomach, and intestines after IN administration. This observation was further confirmed by the *ex vivo* biodistribution study shown in Fig. 1B. Gamma counting found the ^{64}Cu -AuNCs accumulation was significantly higher in the IV group ($n = 4$) than in the IN group ($n = 4$) in the blood ($P < .001$; the ratio of the mean concentrations: IV/IN = 73), lung ($P < .001$; IV/IN = 59), liver ($P < .001$; IV/IN = 12), spleen ($P < .05$; IV/IN = 15), kidney ($P < .001$; IV/IN = 11), and heart ($P < .001$; IV/IN = 79). No statistically significant difference was found in muscle ($P > .05$; IV/IN = 40;), fat ($P > .05$; IV/IN = 37), bone ($P > .05$; IV/IN = 43), marrow ($P > .05$; IV/IN = 18), pancreas ($P > .05$; IV/IN = 15), brain ($P > .05$; IV/IN = 1), and intestine ($P > .05$; IV/IN = 1). Significant higher radioactivity by IN administration was only observed in the stomach ($P < .001$; IN/IV = 8).

3.2. FUSIN enabled noninvasive and localized delivery of AuNCs to the brainstem

Fig. 2A and C are representative autoradiographs of *ex vivo* coronal brain slices from mice treated with IN only and FUSIN, respectively. The corresponding photographs of the slices are presented in Fig. 2B

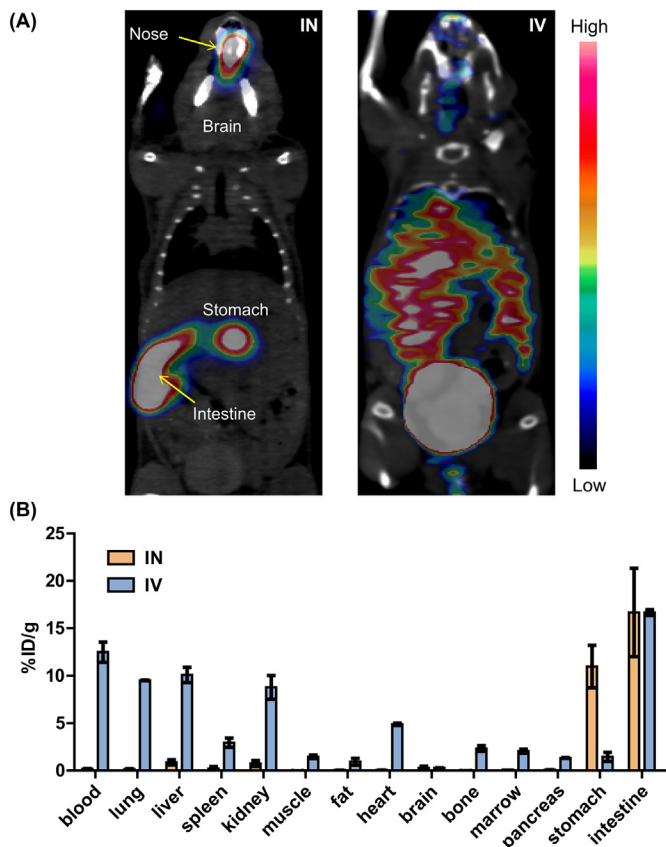


Fig. 1. (A) Representative *in vivo* PET/CT images of mouse whole body coronal view at 1 h after IN administration (left) or IV injection of ⁶⁴Cu-AuNCs (right). (B) Biodistribution of ⁶⁴Cu-AuNCs measured at 1 h post-IN administration (n = 4) or IV injection (n = 4) in different organs as quantified by gamma counting. The IN group showed less radioactivity in most organs than that of the IV group with significantly higher ⁶⁴Cu-AuNCs accumulation observed only in the stomach.

and D to show the anatomical structures of the brain. For the FUSIN-treated mice, FUS was targeted at the left side of the brainstem. Locally enhanced accumulation of ⁶⁴Cu-AuNCs was observed at the FUS-targeted location (Fig. 2C). Quantification of the radioactivity found the radioactivity of ⁶⁴Cu-AuNCs delivered by FUSIN was 2.72 ± 0.79 fold higher than that by IN (Fig. 2E).

Fluorescence imaging of *ex vivo* brain slices from mice administered with TR-AuNCs further confirmed that FUSIN achieved local accumulation of TR-AuNCs at the FUS-targeted location. Fig. 3 shows representative fluorescence images of the FUSIN-treated side of the

brainstem (Fig. 3B) and contralateral non-treated control side (Fig. 3A) from the same brain slice. Strong fluorescence signals were observed in the FUS-treated side of the brainstem with minimal signals observed in the non-treated side. The blood vessels pointed out by arrows in Fig. 3B are highlighted by TR-AuNCs in the perivascular space. Enhanced delivery of TR-AuNCs to the FUS-treated brainstem was consistently found within this group of mice. Quantifications of the fluorescence images revealed a 2.32 ± 1.12-fold enhancement in the fluorescence intensity of TR-AuNCs delivered by FUSIN, compared with IN only.

3.3. FUSIN safety

Fig. 4 displays photographs and corresponding fluorescence images of the mouse nose tissue and trigeminal nerve harvested at 1 h (Fig. 4C and D) and 24 h (Fig. 4E and F) after IN delivery of TR-AuNCs. Mice without TR-AuNCs delivery served as the control (Fig. 4A and B). The nose and trigeminal nerve extracted at 1 h after IN administration exhibited stronger fluorescence signals than those of the control group, confirming that the trigeminal nerve serves as a pathway for IN delivery. At 24 h post IN administration, the intensity of the fluorescence signals was close to the control.

No hemorrhage was observed in the FUSIN-treated brain (Fig. 5B) compared to the control without FUS treatment (Fig. 5A). Nasal sections showed no damage to nasal tissue in the FUSIN TR-AuNCs group (Fig. 5D) compared to the non-treated control group (Fig. 5C). The LFB-CV stained trigeminal nerve sections from both the non-treated control group (Fig. 5E) and FUSIN treated group (Fig. 5F) did not show histological-level changes in the nerve.

4. Discussion

4.1. IN administration minimized systemic exposure

Our study using *in vivo* microPET/CT imaging and *ex vivo* gamma counting confirmed that IN administration of ⁶⁴Cu-AuNCs contributed to minimal systematic exposure (Fig. 1). Quantification of the radioactivity in major organs collected from mice injected with ⁶⁴Cu-AuNCs *via* IV showed > 10-fold uptake in blood, lung, liver, spleen, kidney, and heart than those *via* IN administration. Significant higher radioactivity was only observed in the stomach with IN administration. These findings suggest that ⁶⁴Cu-AuNCs are likely to be removed by mucus to the nasopharynx and accumulated in stomach and intestine [38], which allows the nanoclusters to be excreted from the animal through feces, leading to minimized systemic toxicity of the AuNCs. Previous studies have found consistent results that minimized systemic exposure was associated with IN delivery of larger nanoparticles–micelles (~600 nm) [39]. Here we showed that the small-size AuNCs share the same advantage in minimizing systemic exposure as those larger-size nanoparticles.

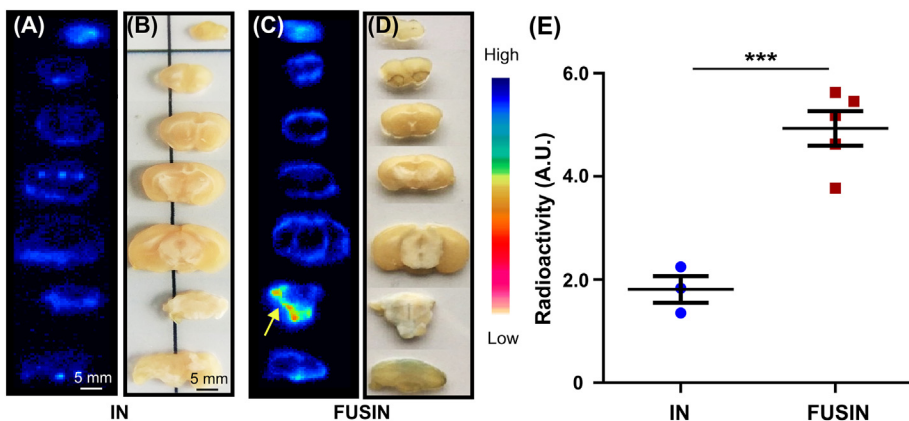


Fig. 2. Representative autoradiographs and corresponding photographs of ⁶⁴Cu-AuNCs in coronal brain slices from mice in the (A, B) IN administration group, and (C, D) FUSIN treatment group, respectively. The arrow in C points to the location where the FUS was targeted for the FUSIN treatment. (E) Quantification of the radioactivity shows statistically significant higher radioactivity was observed in mice treated with FUSIN than IN only (***P < .001).

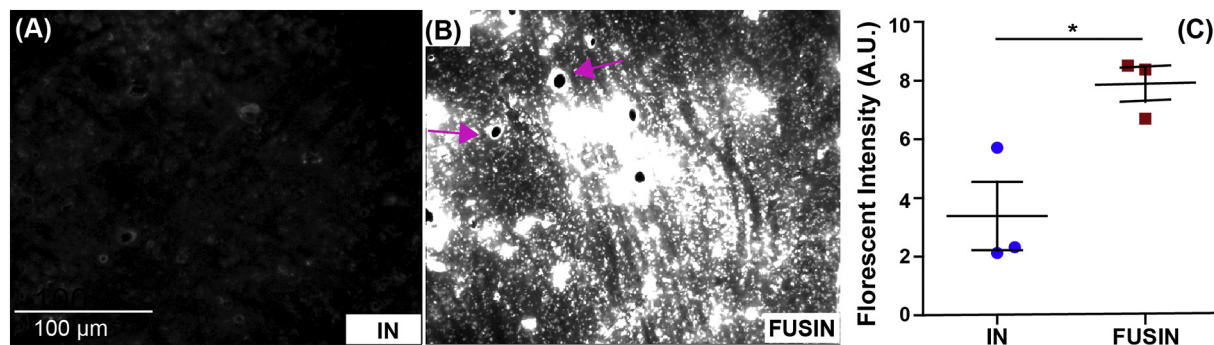


Fig. 3. Representative fluorescence images of a brain slice obtained from a mouse administered with TR-AuNCs followed by FUS treatment on one side of the brainstem (B) and no FUS treatment on the contralateral side of the brainstem (A). The blood vessels are clearly highlighted by the TR-AuNCs in the FUSIN-treated side (arrows). (C) Quantification of the fluorescence intensities found significantly higher fluorescence intensity was observed with FUSIN than IN (* $P < .05$, $n = 3$).

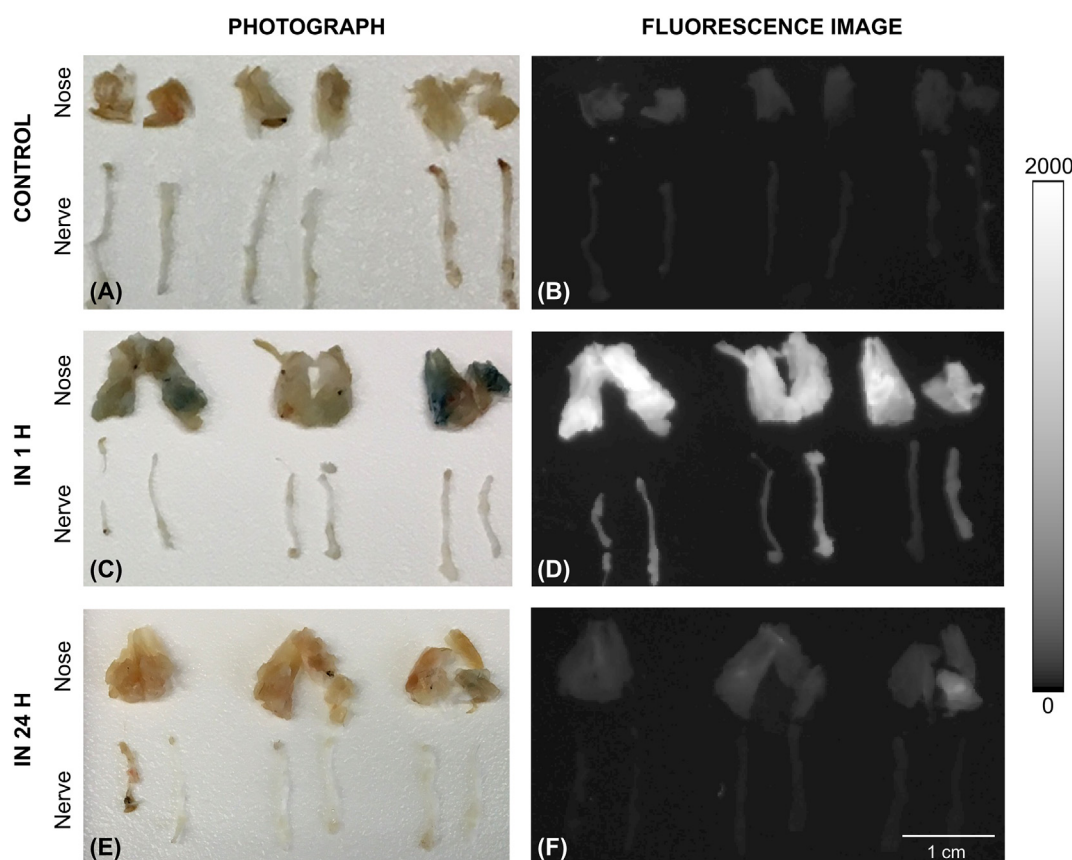


Fig. 4. Photographs and corresponding fluorescence images display the distributions of TR-AuNCs in the nose and trigeminal nerve of mice in the control group (A, B), mice sacrificed 1 h after TR-AuNCs IN administration (C, D), and mice sacrificed 24 h after TR-AuNCs IN administration (E, F). The blue color in the nose tissue in (C) was the color of the TR dye. (For interpretation of the references to color in this figure legend, the reader is referred to the web version of this article.)

4.2. FUSIN for noninvasive and localized delivery of AuNCs

In order to achieve effective drug delivery *via* the nasal route to the brain, innovative designs of nanoparticles were proposed with promising results [5, 22]. However, IN brain drug delivery is still limited by its inefficient and non-localized delivery, which was verified by our data (Figs. 2A and 3A). Integrating IN administration and FUS, we showed locally enhanced delivery of ^{64}Cu -AuNCs and TR-AuNCs to the FUS-targeted brainstem area (Figs. 2C and 3B). The radioactivity of ^{64}Cu -AuNCs delivered by FUSIN and the fluorescence intensity of TR-AuNCs delivered by FUSIN were both more than two-fold higher than that of IN only (Figs. 2E and 3C). Previous studies on IN brain drug delivery concentrated on enhancing the agent absorption across the

nasal epithelium to improve the IN delivery efficiency to the brain [15, 34, 35]. This study showed that IN delivery efficiency can be improved by FUSIN, which enhanced the accumulation of IN administered agents by inducing microbubble cavitation at the desired brain location. Meanwhile, the capability of FUSIN in localized nanoparticle delivery makes it possible to achieve therapeutic drug level only within the targeted site while keeping non-targeted sites at the sub-therapeutic level, thus minimizing any potential side effects to healthy regions of the brain. It is noted that the quantification of radioactivity and fluorescence intensity was an indirect estimation of the AuNC delivery efficiency. Future study is needed to provide direct quantification of the AuNC delivery efficiency in terms of %ID or %ID/g using methods such as inductively coupled plasma mass spectrometry (ICP-MS) to directly

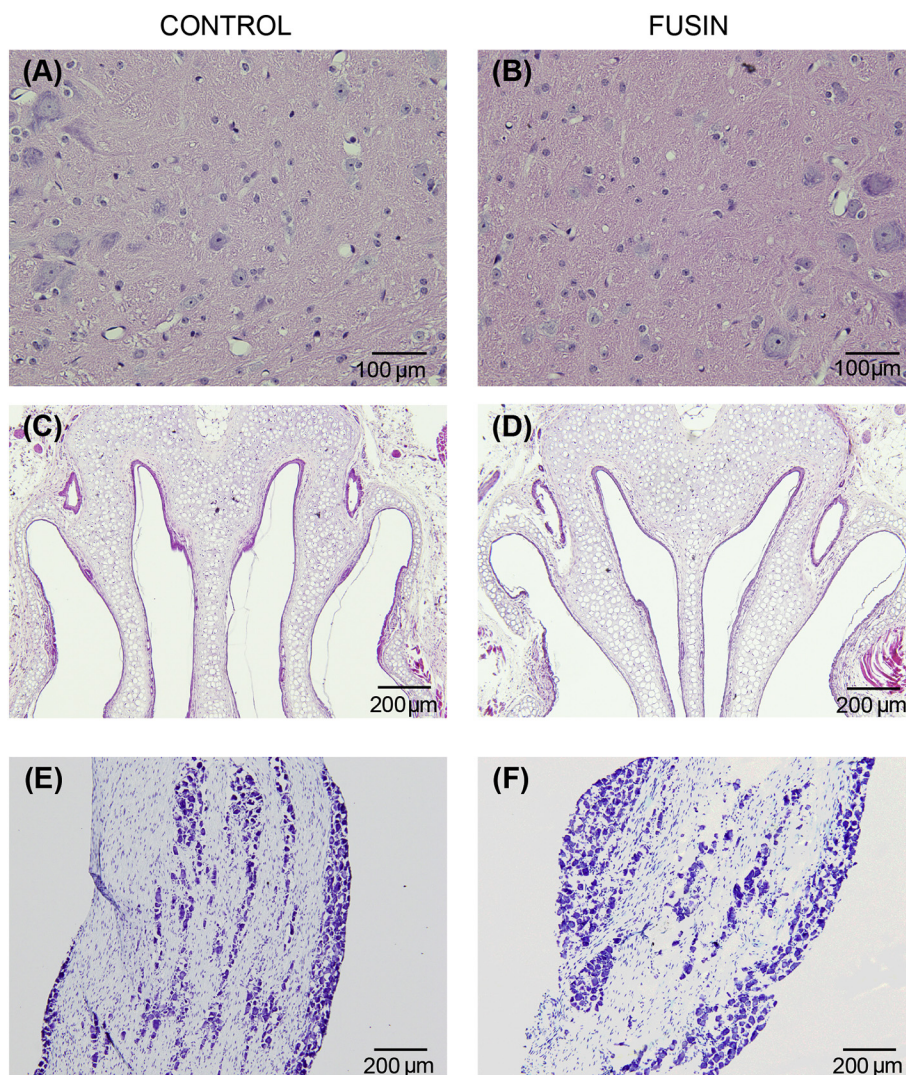


Fig. 5. Histological examinations by H&E staining of (A) the non-sonicated and (B) the contralateral FUS-sonicated brainstem reveal no hemorrhage associated with the FUS treatment. H&E staining of the nasal sections from (C) the control mice without agent delivery and (D) the mice with IN administered TR-AuNCs found no damage to the nasal tissue by IN administration. The LFB-CV staining of trigeminal nerves from (E) the non-treated control mice and (F) the mice with IN administration of TR-AuNCs shows IN administration of AuNCs did not cause histological-level damage to the nerve tissue.

measure the Au concentrations.

Previous studies have shown that FUSIN noninvasively enhanced the localized delivery of fluorescently labeled dextran (40 kDa) and BDNF (27 kDa) to the caudate putamen of mouse brains [5, 22]. These previous findings, combined with our current results, suggest that FUSIN is a promising platform technology for delivering different types of agents to different brain locations. Future studies are needed to compare the delivery efficiencies of different agents to the same targeted brain location to evaluate the dependency of the FUSIN delivery efficiency on the types of the therapeutic agents, as well as to compare the delivery efficiency of the same agent to different locations to assess the location-dependency of FUSIN.

It is worthwhile to point out that FUSIN relies on the same mechanical interactions among FUS, microbubbles, and microvessels as the conventional FUS-induced BBB opening technique. AuNCs that entered the blood circulation through IN-administration may be delivered from the blood circulation to the brain parenchyma through the BBB. However, the level of AuNCs in the blood after IN administration was minimal, with a concentration 73-fold lower than that after IV administration (Fig. 1B). This finding is consistent with previous studies showing that IN delivered agents were directly transported from the nose to the brain through the olfactory nerve and trigeminal nerve

pathways with minimal amounts entering the blood circulation [6, 8, 39, 40]. This finding suggests that the enhanced delivery observed in the brain by FUSIN was mainly due to the contribution of the nose-to-brain pathway instead of the blood-to-brain pathway.

4.3. Safety of FUSIN

Extensive research has demonstrated the safety of IN administration [41], which justifies IN brain drug delivery studies in animals and early-phase clinical trials. The IN administration method that we used in this study followed a standard protocol for mice that have been used by several other groups [15, 21]. To verify the safety of IN administration, we performed H&E staining of the nasal tissue obtained from mice treated by IN administration of TR-AuNCs and found no changes in the nasal tissue compared with the control group (Fig. 5C and D).

The enhanced fluorescence signals observed in the fluorescence images of the trigeminal nerve at 1 h confirmed that the trigeminal nerve is a pathway for IN delivery to the brainstem. The fluorescence image acquired at 24 h post IN administration of TR-AuNCs (Fig. 4F) showed a fluorescence intensity close to that of the control (Fig. 4B), suggesting clearance of the nanoparticles from the nerve. No change was observed by comparison of the stained trigeminal nerves from mice

treated by FUSIN and those from the non-treated control group (Fig. 5E and F).

Since the brainstem coordinates motor control signals to the body and controls life supporting autonomic functions of the peripheral nervous system, the parameters of FUS were carefully chosen in reference to previous FUS-induced BBB opening studies to avoid hemorrhage or neuron damage [37, 42]. As expected, these parameters did not cause any vascular or tissue damage at the FUS targeted brainstem region (Fig. 5B). Although not the focus of this study, we closely observed the mice behavior until the animals fully recovered from anesthesia. All treated mice recovered from anesthesia within 15 min after the FUS treatment. After recovery, no gross behavior change was observed in drinking, eating, walking, hanging, jumping, or grooming.

4.4. Limitations of this study

There are several major limitations of this study. First, the treatment timeline and FUS parameters were not optimized. The FUS treatment parameters were selected in reference to previous studies of the FUS-induced BBB opening technique. Future studies must refine these parameters to improve the delivery efficiency of FUSIN. Meanwhile, *ex vivo* autoradiography and fluorescence imaging were used to assess the AuNCs distribution in the mouse brain. Future studies are needed to determine the pharmacokinetics of the AuNCs using *in vivo* PET/CT imaging in order to reveal the spatiotemporal kinetics of AuNCs delivered by FUSIN. The safety evaluation of FUSIN was performed after a single treatment within a short-term period (1 h after treatment). Future studies are needed to evaluate the long-term safety of FUSIN, especially after repeated treatments. Moreover, we used AuNCs with only one size in this study. Future studies will optimize the design of the AuNCs, such as size and surface charge, to optimize the FUSIN delivery outcome. Last but not least, we showed minimized exposure of the AuNCs to major organs, but we did not systemically evaluate the toxicity of the AuNCs. Future studies are needed to systemically evaluate the safety of AuNCs, including hepatotoxicity, hematological toxicity, and inflammatory response to fully demonstrate the advantage of FUSIN in minimizing nanoparticle toxicity.

5. Conclusions

Brain drug delivery is not only challenged by the limited delivery efficiency due to the existence of the BBB but also the need to reduce systemic toxicity. This study showed the advantage of IN administration of AuNCs in minimizing systemic exposure compared with systemic injection. It found that FUSIN achieved localized and enhanced delivery of AuNCs compared with IN brain drug delivery. A short-term safety evaluation of FUSIN-treated mice did not find histological-level tissue damage to the nose, trigeminal nerve, and brain. These findings suggest that FUSIN is a promising technique for noninvasive, spatially targeted, and safe delivery of nanoparticles to the brain with minimal systemic exposure.

Declaration of interest

None.

Acknowledgments

This work was supported by a grant from the American Cancer Society [grant number IRG-58-010-61-1]. It was also supported by the Children's Discovery Institute of Washington University and St. Louis Children's Hospital [grant number MC-II-2017-661]. Ramesh Raliya was partially supported by the CMMN Grant NIH-NCI U54CA199092. We thank Prof. Rajiv Chopra and Ms. Chenchen Bing from the University of Texas Southwestern for providing us with the ultrasound transducer and technical assistance in setting up the second ultrasound system used in this study.

References

- [1] W.M. Pardridge, The blood-brain barrier: Bottleneck in brain drug development, *NeuroRx* 2 (2005) 3–14.
- [2] M.M. Patel, B.M. Patel, Crossing the blood–brain barrier: recent advances in drug delivery to the brain, *CNS Drugs* 31 (2017) 109–133.
- [3] K. Hynynen, N. McDannold, N. Vykhotseva, F.A. Jolesz, Noninvasive MR imaging-guided focal opening of the blood-brain barrier in rabbits, *Radiology* 220 (2001) 640–646.
- [4] M. Aryal, C.D. Arvanitis, P.M. Alexander, N. McDannold, Ultrasound-mediated blood-brain barrier disruption for targeted drug delivery in the central nervous system, *Adv. Drug Deliv. Rev.* 72 (2014) 94–109.
- [5] H. Chen, C.C. Chen, C. Acosta, S.-Y. Wu, T. Sun, E.E. Konofagou, A new brain drug delivery strategy: focused ultrasound-enhanced intranasal drug delivery, *PLoS One* 9 (2014) e108880.
- [6] J.J. Lochhead, R.G. Thorne, Intranasal delivery of biologics to the central nervous system, *Adv. Drug Deliv. Rev.* 64 (2012) 614–628.
- [7] H.V. Dhuria, L.R. Hanson, W.H. Frey, Intranasal delivery to the central nervous system: mechanisms and experimental considerations, *Int. J. Drug Dev. Res.* 3 (2011) 26–33.
- [8] R.G. Thorne, G.J. Pronk, V. Padmanabhan, W.H. Frey, Delivery of insulin-like growth factor-I to the rat brain and spinal cord along olfactory and trigeminal pathways following intranasal administration, *Neuroscience* 127 (2004) 481–496.
- [9] N. Nonaka, S.A. Farr, H. Kageyama, S. Shioda, W.A. Banks, Delivery of galanin-like peptide to the brain: targeting with intranasal delivery and cyclodextrins, *J. Pharmacol. Exp. Ther.* 325 (2008) 513–519.
- [10] A. Kumral, B. Iscan, D. Engur, F. Tuzun, S. Ozbal, B.U. Ergur, M. Kaynak Turkmen, N. Duman, H. Ozkan, Intranasal surfactant protein D as neuroprotective rescue in a neonatal rat model of periventricular leukomalacia, *J. Mater. Neonatal Med.* 30 (2017) 446–451.
- [11] G. Rassa, E. Soddu, A.M. Posadino, G. Pintus, B. Sarmiento, P. Giunchedi, E. Gavini, Nose-to-brain delivery of BACE1 siRNA loaded in solid lipid nanoparticles for Alzheimer's therapy, *Colloids Surf. B Biointerf.* 152 (2017) 296–301.
- [12] X. Zhuang, Y. Teng, A. Samykutty, J. Mu, Z. Deng, L. Zhang, P. Cao, Y. Rong, J. Yan, D. Miller, H.-G. Zhang, Grapefruit-derived nanovectors delivering therapeutic miR17 through an intranasal route inhibit brain tumor progression, *Mol. Ther.* 24 (2015) 96–105.
- [13] C. Benedict, M. Hallschmid, A. Hatke, B. Schultes, H.L. Fehm, J. Born, W. Kern, Intranasal insulin improves memory in humans, *Psychoneuroendocrinology* 29 (2004) 1326–1334.
- [14] C. Benedict, M. Hallschmid, K. Schmitz, B. Schultes, F. Ratter, H.L. Fehm, J. Born, W. Kern, Intranasal insulin improves memory in humans: superiority of insulin aspart, *Neuropsychopharmacology* 32 (2007) 239–243.
- [15] M. Krishan, G. Gudelsky, P.B. Desai, M.B. Genter, Manipulation of olfactory tight junctions using papaverine to enhance intranasal delivery of gemcitabine to the brain, *Drug Deliv.* 21 (2014) 8–16.
- [16] Y.-Z. Zhao, M. Lin, Q. Lin, W. Yang, X.-C. Yu, F.-R. Tian, K.-L. Mao, J.-J. Yang, C.-T. Lu, H.L. Wong, Intranasal delivery of bFGF with nanoliposomes enhances *in vivo* neuroprotection and neural injury recovery in a rodent stroke model, *J. Control. Release* 224 (2016) 165–175.
- [17] B. Bernocchi, R. Carpentier, I. Lantier, C. Ducournau, I. Dimier-Poisson, D. Betbeder, Mechanisms allowing protein delivery in nasal mucosa using NPL nanoparticles, *J. Control. Release* 232 (2016) 42–50.
- [18] E. Muntimadugu, R. Dhommatti, A. Jain, V.G.S. Challa, M. Shaheen, W. Khan, Intranasal delivery of nanoparticle encapsulated tarenflurbil: A potential brain targeting strategy for Alzheimer's disease, *Eur. J. Pharm. Sci.* 92 (2016) 224–234.
- [19] L. Illum, Is nose-to-brain transport of drugs in man a reality, *J. Pharm. Pharmacol.* 56 (2004) 3–17.
- [20] A. Mistry, S. Stolnik, L. Illum, Nanoparticles for direct nose-to-brain delivery of drugs, *Int. J. Pharm.* 379 (2009) 146–157.
- [21] P. JR, J. M, A. A, J. MP, C. H, F.D. Boussin, Intranasal administration of temozolomide delayed the development of brain tumors initiated by human glioma stem-like cell in nude mice, *J. Cancer Sci. Ther.* 9 (2017) 374–378.
- [22] H. Chen, G.Z.X. Yang, H. Getachew, C. Acosta, C. Sierra Sánchez, E.E. Konofagou, Focused ultrasound-enhanced intranasal brain delivery of brain-derived neurotrophic factor, *Sci. Rep.* 6 (2016) 28599.
- [23] H. Chen, W. Kreider, A.A. Brayman, M.R. Bailey, T.J. Matula, Blood vessel deformations on microsecond time scales by ultrasonic cavitation, *Phys. Rev. Lett.* 106 (2011) 34301.
- [24] H.S. Choi, W. Liu, P. Misra, E. Tanaka, J.P. Zimmer, B. Itty Ipe, M.G. Bawendi, J.V. Frangioni, Renal clearance of nanoparticles, *Nat. Biotechnol.* 25 (2007) 1165–1170.
- [25] T. Chen, S. Xu, T. Zhao, L. Zhu, D. Wei, Y. Li, H. Zhang, C. Zhao, Gold nanocluster-conjugated amphiphilic block copolymer for tumor-targeted drug delivery, *ACS Appl. Mater. Interfaces* 4 (2012) 5766–5774.
- [26] M. Longmire, P.L. Choyke, H. Kobayashi, Clearance properties of nano-sized particles and molecules as nanomedicine, *Nanomedicine* 3 (2008) 703–717.
- [27] X.D. Zhang, D. Wu, X. Shen, P.X. Liu, F.Y. Fan, S.J. Fan, *In vivo* renal clearance, biodistribution, toxicity of gold nanoclusters, *Biomaterials* 33 (2012) 4628–4638.
- [28] Y. Zhao, D. Sultan, L. Detering, H. Luehmann, Y. Liu, Facile synthesis, pharmacokinetic and systemic clearance evaluation, and positron emission tomography cancer imaging of ⁶⁴Cu–Au alloy nanoclusters, *Nanoscale* 6 (2014) 13501–13509.
- [29] Y. Zhao, L. Detering, D. Sultan, M.L. Cooper, M. You, S. Cho, S.L. Meier, H. Luehmann, G. Sun, M. Rettig, F. Dehdashti, K.L. Wooley, J.F. Dipersio, Y. Liu, Gold nanoclusters doped with ⁶⁴Cu for CXCR4 positron emission tomography

- imaging of breast cancer and metastasis, *ACS Nano* 10 (2016) 5959–5970.
- [30] L.M. Hirvonen, G.O. Fruhwirth, N. Srikantha, M.J. Barber, J.E. Neffendorf, K. Suhling, T.L. Jackson, Hydrodynamic radii of ranibizumab, aflibercept and bevacizumab measured by time-resolved phosphorescence anisotropy, *Pharm. Res.* 33 (2016) 2025–2032.
- [31] D. Hargrave, U. Bartels, E. Bouffet, Diffuse brainstem glioma in children: Critical review of clinical trials, *Lancet Oncol.* 7 (2006) 241–248.
- [32] J. Tisnado, R. Young, K.K. Peck, S. Haque, Conventional and advanced imaging of diffuse intrinsic pontine glioma, *J. Child Neurol.* 31 (2016) 1386–1393.
- [33] D. Ye, D. Sultan, X. Zhang, Y. Yue, G.S. Heo, S.V.V.N. Kothapalli, H. Luehmann, Y. chuan Tai, J.B. Rubin, Y. Liu, H. Chen, Focused ultrasound-enabled delivery of radiolabeled nanoclusters to the pons, *J. Control. Release* 283 (2018) 143–150.
- [34] C. Bing, M. Ladouceur-Wodzak, C.R. Wanner, J.M. Shelton, J.A. Richardson, R. Chopra, Trans-cranial opening of the blood-brain barrier in targeted regions using a stereotaxic brain atlas and focused ultrasound energy, *J. Ther. Ultrasound* 2 (2014) 13.
- [35] T.C. Rainbow, B. Parsons, B.B. Wolfe, Quantitative autoradiography of beta 1- and beta 2-adrenergic receptors in rat brain, *Proc. Natl. Acad. Sci. U. S. A.* 81 (1984) 1585–1589.
- [36] R. Raliya, D. Saha, T.S. Chadha, B. Raman, P. Biswas, Non-invasive aerosol delivery and transport of gold nanoparticles to the brain, *Sci. Rep.* 7 (2017) 44718.
- [37] H. Chen, E.E. Konofagou, The size of blood-brain barrier opening induced by focused ultrasound is dictated by the acoustic pressure, *J. Cereb. Blood Flow Metab.* 34 (2014) 1197–1204.
- [38] S. Savale, H. Mahajan, Nose to brain: A versatile mode of drug delivery system, *Asian J. Biomater. Res.* 3 (2017) 16–38.
- [39] H.M. Rashed, R.N. Shamma, E.B. Basalious, Contribution of both olfactory and systemic pathways for brain targeting of nimodipine-loaded lipo-pluronic micelles: In vitro characterization and in vivo biodistribution study after intranasal and intravenous delivery, *Drug Deliv.* 24 (2017) 181–187.
- [40] F. Sonvico, A.R. Clementino, F. Buttini, G. Colombo, Surface-modified nanocarriers for nose-to-brain delivery: From bioadhesion to targeting, *Pharmaceutics* 10 (2018) 34.
- [41] J. Wang, W.L. Lu, G.W. Liang, K.C. Wu, C.G. Zhang, X. Zhang, J.C. Wang, H. Zhang, X.Q. Wang, Q. Zhang, Pharmacokinetics, toxicity of nasal cilia and immunomodulating effects in Sprague-Dawley rats following intranasal delivery of thymopentin with or without absorption enhancers, *Peptides* 27 (2006) 826–835.
- [42] B. Baseri, J.J. Choi, Y.-S. Tung, E.E. Konofagou, Multi-modality safety assessment of blood-brain barrier opening using focused ultrasound and definity microbubbles: A short-term study, *Ultrasound Med. Biol.* 36 (2010) 1445–1459.